Combined Metabonomic and Quantitative Real-Time PCR Analyses Reveal Systems Metabolic Changes of Fusarium graminearum Induced by Tri5 Gene Deletion

ARTICLE *in* JOURNAL OF PROTEOME RESEARCH · MARCH 2011

Impact Factor: 4.25 · DOI: 10.1021/pr101095t · Source: PubMed

7 AUTHORS, INCLUDING:

Fangfang Chen
Chinese Academy of Sciences
5 PUBLICATIONS **73** CITATIONS
SEE PROFILE

Jingtao Zhang
Chinese Academy of Sciences
11 PUBLICATIONS **158** CITATIONS
SEE PROFILE

Huiru Tang
Fudan University
167 PUBLICATIONS **4,950** CITATIONS
SEE PROFILE

Journal of proteome research

ARTICLE

pubs.acs.org/jpr

Combined Metabonomic and Quantitative Real-Time PCR Analyses Reveal Systems Metabolic Changes of *Fusarium graminearum* Induced by *Tri5* Gene Deletion

Fangfang Chen,[†,#] Jingtao Zhang,[‡,§,#] Xiushi Song,[†] Jian Yang,[†] Heping Li,[†] Huiru Tang,[*,‡] and Yu-Cai Liao[*,†,∥,⊥]

[†]Molecular Biotechnology Laboratory of Triticeae Crops, Huazhong Agricultural University, Wuhan 430070, P.R. China

[‡]State Key Laboratory of Magnetic Resonance and Atomic and Molecular Physics, Wuhan Centre for Magnetic Resonance, Wuhan Institute of Physics and Mathematics, the Chinese Academy of Sciences, Wuhan 430071, P.R. China

[§]Graduate School of Chinese Academy of Sciences, Beijing 100049, P.R. China

[∥]College of Plant Science and Technology, Huazhong Agricultural University, Wuhan 430070, P.R. China

[⊥]National Center of Plant Gene Research (Wuhan), Wuhan 430070, P.R. China

Supporting Information

ABSTRACT: *Fusarium graminearum* (FG) is a serious plant pathogen causing huge losses in global production of wheat and other cereals. *Tri5*-gene encoded trichodiene synthase is the first key enzyme for biosynthesis of trichothecene mycotoxins in FG. To further our understandings of FG metabolism which is essential for developing novel strategies for controlling FG, we conducted a comprehensive investigation on the metabolic changes caused by *Tri5*-deletion by comparing metabolic differences between the wild-type FG5035 and an FG strain, *Tri5*$^{-}$, with *Tri5* deleted. NMR methods identified more than 50 assigned fungal metabolites. Combined metabonomic and quantitative RT-PCR (qRT-PCR) analyses revealed that *Tri5* deletion caused significant and comprehensive metabolic changes for FG apart from mycotoxin biosynthesis. These changes involved both carbon and nitrogen metabolisms including alterations in GABA shunt, TCA cycle, shikimate pathway, and metabolisms of lipids, amino acids, inositol, choline, pyrimidine, and purine. The hexose transporter has also been affected. These findings have shown that *Tri5* gene deletion induces widespread changes in FG primary metabolism and demonstrated the combination of NMR-based metabonomics and qRT-PCR analyses as a useful way to understand the systems metabolic changes resulting from a single specific gene knockout in an eukaryotic genome and thus *Tri5* gene functions.

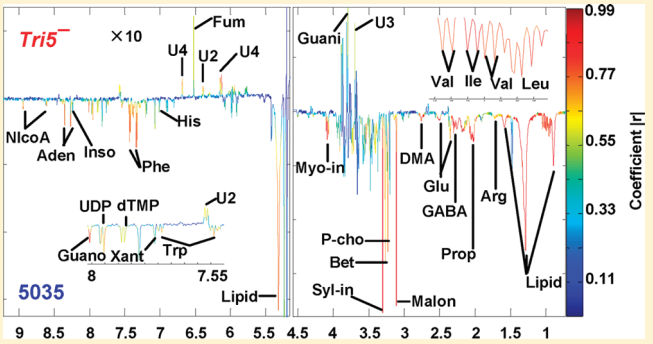

KEYWORDS: ^{1}H NMR, *Tri5* gene, metabonomics, *Fusarium graminearum*, quantitative real-time PCR

INTRODUCTION

Fusarium head bight (FHB) caused by *Fusarium graminearum* (FG) infection is a serious plant disease affecting wheat and other cereal (e.g., maize) productions globally. Since the mid-1990s, FHB has re-emerged as a serious problem to agriculture in North America and Europe[1−4] and is considered the worst plant disease in the U.S. Between 1998 and 2000, FHB caused losses in the U.S. alone were estimated to be about 3 billion U.S. dollars.[5−7] Global climate changes during recent years have aggravated the spread and severity of FHB to even wider regions, and thus, FHB is now considered as one of the most adverse factors for the global cereal productions.[1] Furthermore, since FG produces various trichothecene mycotoxins that are toxic to human and domestic animals,[8,9] its infection ruins almost all cereals produced in the affected fields with unusable products. Comprehensive understanding of the mechanistic aspects of FG toxin biosynthesis and infections to cereals is vitally important for developing FG-resistant plants and other novel strategies to achieve effective controls of *Fusarium* mycotoxins in food/feed chains.

Chemical and molecular aspects of trichothecene mycotoxin biosynthesis pathways in *Fusarium* species has been well studied in terms of the mycotoxin intermediates and gene clusters as well as their regulations.[10−14] Previous studies have found that the *Tri5* gene of FG encodes the first key enzyme, trichodiene synthase, responsible for the biosynthesis of trichothecene mycotoxins. These toxins are sesquiterpenes and secondary metabolites of *Fusarium* species including deoxynivalenol (DON), nivalenol (NIV), T2 and their derivatives. Trichodiene

Received: October 30, 2010
Published: February 28, 2011

synthase catalyzes farnesyl pyrophosphate (FPP) through cyclization to form trichodiene (TDN) that serves as the first intermediate entering into thichothecene mycotoxin biosynthesis,[15,16] although FPP is actually a common intermediate in the biosynthesis of various secondary metabolites.[17] Deleting *Tri5* gene in a DON-producing *F. graminearum* strain completely abolished the mycotoxin production and caused a reduction of virulence on plants.[18,19] In nature, DON producing *Fusarium* species are self-protected from the DON toxicity as the fungi carry a *Tri101* gene encoding trichothecene 3-*O*-acetyltranferase to acetylate the mycotoxins at C-3 position.[20]

More recently, the basal metabolism differences between four wild-type *Fusarium* spp. were thoroughly studied[21] using ^{1}H nuclear magnetic resonance (NMR) and direct-injection electrospray ionization-mass spectroscopy. The nutritional environment was found to have a greater influence on the fungal metabonome than their genotypes.[21] However, the effects of *Tri5* deletion on the metabolic processes of *F. graminearum* (other than mycotoxin biosynthesis) remain to be fully understood. Metabonomic analysis ought to be suitable to acquire such needed information since metabonomics is a branch of science dealing with the metabolite compositions of biological systems and their responses to the changes of both endogenous and exogenous factors.[22,23] Such approaches have already found widespread successful applications in understanding the effects of toxins[24−26] and stresses,[27−30] pathogenesis,[31−33] and in molecular phenotyping.[34]

In this study, we systematically investigated the metabolic differences between wild-type *F. graminearum* strain 5035 and FG strain with the *Tri5* gene deleted, *Tri5*$^-$, using the NMR-based metabonomics methods. Quantitative real-time PCR (qRT-PCR) analyses were further employed to measure expressions of 25 relevant genes together with the production of DON and 15-acetyldeoxynivalenol (15-ADON) to obtain complementary information. The objectives of this study are to further characterize the features of metabolite composition (metabonome) for *F. graminearum* and define the effects of *Tri5* deletion on metabolisms of this fungal species so as to provide more information for the functions of *Tri5* gene.

MATERIALS AND METHODS

Methanol, sodium chloride, $K_2HPO_4 \cdot 3H_2O$, and $NaH_2PO_4 \cdot 2H_2O$ (all in analytical grade) purchased from Guoyao Chemical Co. Ltd. (Shanghai, China) were used without further purification. D_2O (99.9% D) and sodium 3-trimethlysilyl [2,2,3,3-D_4] propionate (TSP) were purchased from Cambridge Isotope Laboratories (Miami, FL) with the latter used as a chemical shift reference. Phosphate buffer solution of $NaH_2PO_4-K_2HPO_4$ (0.1 M, pH7.4) was prepared in H_2O (with 10% D_2O, 0.02% TSP) and used for NMR studies owing to good solubility and low temperature stability.[35]

Fungus Materials and Culture

F. graminearum strain 5035 isolated from a scabby wheat spike in Wuhan, China, is a deoxynivalenol (DON)-producer and highly pathogenic in wheat.[36,37] An isogenic strain with the *Tri5* gene deleted, *Tri5*$^-$, was made from the above wild type through homologous recombination via *Agrobacterium*-mediated transformation.[38] The morphology and growth rate of hyphae of the strains 5035 and *Tri5*$^-$ were studied as previously described.[39] Molecular characterization confirmed this strain with a specific deletion of the *Tri5* gene encoding trichodiene synthase[38] catalyzing farnesyl pyrophosphate to form trichodiene that is the precursor for biosynthesis of trichothecene mycotoxins, including DON, NIV, T2, and their various derivatives.[15,16] *Fusarium* strains were cultured in CMC broth[40] at 28 °C (200 rpm) for 5 days. Conidiaspores were collected and adjusted to a concentration of 1×10^6 spores/mL. An aliquot of 10 μL droplet of the conidia was inoculated on sterile glass-membrane paper over potato-dextrose agar (PDA) at 28 °C for 3 days. The harvested mycelium was snap-frozen in liquid nitrogen, grounded to powder, lyophilized, and stored at −80 °C until further analysis. The harvested samples were divided into two parts for NMR-base metabonomic analysis and RNA extraction, respectively. Trichothecene mycotoxins from two strains, the wild-type FG5035 and *Tri5*$^-$, were extracted and determined with GC−MS methods as previously described.[41] Commercial trichothecene mycotoxins, DON, 3-acetyldeoxynivalenol (3-ADON), 15-ADON, NIV, fusarenon-X (FX), and T2 purchased from Sigma were used as standards during determination by GC−MS. In metabonomic analysis, 18 biological replicates were used for *F. graminearum* strains 5035 and *Tri5*$^-$, whereas three independent biological samples were employed for quantitative real time PCR measurements.

Metabolite Extraction Procedures of Fungal Samples

Freeze-dried powder samples (ca. 25 mg) of each strain were transferred into a microtube (2 mL) with addition of 1.2 mL of precooled methanol/water (2/1; v/v, −40 °C). Mixtures were then extracted by intermittent sonication (i.e., 30 s sonication with 30 s break) for 10 min in an ice bath. Following centrifugation (16 000*g*, 4 °C) for 10 min, the supernatant from each sample was transferred into a new microtube (5 mL) and the remaining solid residues were further extracted twice using the same procedure. Methanol was removed under vacuum with a Speed-Vac Concentrator (Thermo SAVANT, SC110A-230) from the combined supernatant from three extractions. The supernatants were then lyophilized in a freeze-drier which took at least 24 h. Two blanks were added in parallel to the entire extraction processes. The extracts were dissolved into 550 μL of phosphate buffer (0.1 M, pH 7.4) containing 10% D_2O (v/v) and 0.02% TSP and centrifuged for 10 min. A total of 500 μL of supernatant of each sample was then transferred into 5 mm NMR tubes for NMR analysis.

NMR Measurements

^{1}H NMR spectra were recorded at 298 K on a Bruker AV III 600 NMR spectrometer equipped with a 5-mm inverse TXI cryogenic probe (Bruker Biospin, Germany) operating at 600.13 MHz for ^{1}H. A one-dimensional NOESY-based pulse sequence [*RD*-90°-t_1-90°-t_m-90°-acquisition][26,34] was used to obtain metabolic profiles of fungal extracts with 90° pulse length of about 9.5 μs. t_1 was set to 3 μs. Water suppression was achieved with a weak irradiation during recycle delay (*RD*, 2 s) and mixing time (t_m, 100 ms). A total of 64 transients were collected into 32 768 data points for each spectrum with a spectral width of 12 kHz, and acquisition time was 1.36 s. All spectra were recorded within 8 h with each sample in solution for less than 1 h. An exponential window function with line broadening factor of 0.5 Hz was applied to all free induction decays (FIDs) prior to Fourier transformation (FT). The chemical shifts were referenced to TSP at δ 0.00.

For assignment purposes, ^{1}H−^{1}H COSY, TOCSY, ^{1}H−^{13}C HSQC, and HMBC 2D NMR spectra were recorded as previously reported[28,34] for selected fungal extracts. Briefly, for

COSY and TOCSY experiments, 16 transients were collected into 2K data points for each of 128 increments with spectral width of 10.5 ppm in both dimensions. TOCSY 2D NMR spectra were acquired with MLEV-17 as the spin−lock scheme and the mixing time of 80 ms. The data were zero-filled into 2K data points in both dimensions and a sine window function was applied to the free induction decay prior to FT. $^{1}H-^{13}C$ HSQC 2D NMR spectra were acquired into 2K data points in an echo−antiecho mode using the gradient selected sequence with 32 transients for each of 220 increments. The spectral widths were 6313 Hz in the ^{1}H dimension and 26410 Hz in the ^{13}C dimension. $^{1}H-^{13}C$ HMBC 2D NMR spectra were acquired into 2K data points in a phase-insensitive mode using the gradient selected sequence with 100 transients for each of 200 increments. The spectral widths were 6313 Hz in the ^{1}H dimension and 33957 Hz in the ^{13}C dimension. The data were zero-filled to 2K and a sinebell-squared function was applied to the FID, in both dimensions, prior to FT.

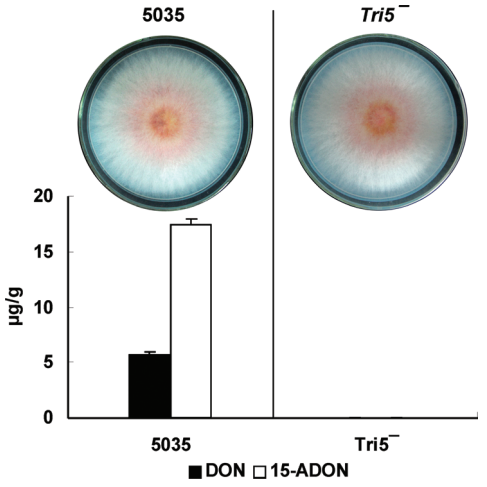

Figure 1. Morphology (top panel) and mycotoxin productions (bottom panel) for two *F. graminearum* strains 5035 and *Tri5*$^{-}$.

Data Treatment and Multivariate Data Analysis

Following phase- and baseline-corrections for all ^{1}H NMR spectra with TOPSPIN (v2.1, Bruker Biospin GmbH, Germany), the region of δ0.5−9.5 ppm was divided into bins with width of 0.003 ppm (1.8 Hz) using the AMIX software (v 3.8.3, Bruker Biospin GmbH, Germany). The region at δ 4.53−5.15 ppm was discarded to remove the effects of imperfect water presaturation. The areas of remaining bins were normalized to the weight of extracts used. Principal component analysis (PCA) was carried out on the mean-centered NMR data using the software package SIMCA-P+ (v 11.0, Umetrics, Sweden) to inspect overall data distributions, possible outliers, and potentially altered metabolites (Supporting Information Figure S1). The orthogonal signal correction projection to latent structure discriminant analysis (OPLS-DA) was further performed (using the same software) with unit variance scaling (UV) using the NMR data as the **X**-matrix and group information as **Y**-matrix.[29,42] Such a model was calculated with one orthogonal and one predictive component. The results were presented in the forms of scores plots with each point representing the metabolite composition (metabonome) of each sample and loadings plots where data points represented variables (metabolites) contributing to group classifications.

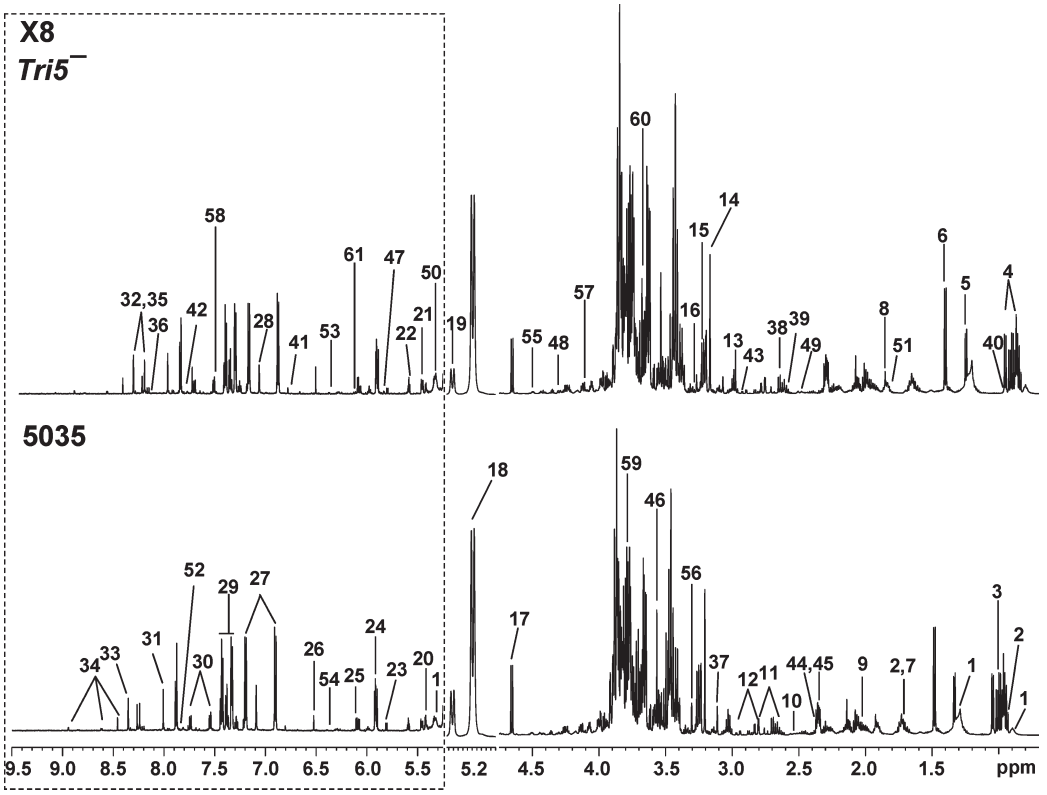

Figure 2. The 600 MHz ^{1}H NMR spectra of fungal extracts from *F. graminearum* strains 5035 and *Tri5*$^{-}$. The spectra δ 9.5−5.25 (in the dotted box) was vertically expanded 8 times. The key numbers are listed in Table 1.

dx.doi.org/10.1021/pr101095t |J. Proteome Res. 2011, 10, 2273–2285

Table 1. Metabolite Assignments of NMR Data for *F. graminearum* Strains 5035 and *Tri5*$^-$

no.	metabolites	group	δ ^{1}H (multiplicity)[a]	δ ^{13}C	experiments
1	lipid	CH_3	0.89 (m)	17.1	TOCSY, HSQC
		$(CH_2)_n$	1.27 (m)	32.7	
		CH═CH	5.33 (m)	132.5	
2	leucine	δ-CH_3	0.96 (t, 6.6 Hz)	23.9	TOCSY, HSQC, HMBC
		δ'-CH_3	0.94 (t, 7.4 Hz)	26.7	
		γ-CH	1.69 (m)	26.9	
		β-CH_2	1.72 (m)	42.8	
		α-CH	3.69 (t, 9.5 Hz)	56.4	
3	isoleucine	γ'-CH_3	1.01 (d, 7.0 Hz)	17.7	TOCSY, HSQC, HMBC
		δ-CH_3	0.94 (t, 7.4 Hz)	14.1	
		γ-CH_2	1.25 (m)	27.3	
		β-CH	1.96 (m)	38.8	
		α-CH	3.65 (m)	62.4	
4	valine	γ-CH_3	1.04 (d, 7.0 Hz)	21.1	TOCSY, HSQC, HMBC
		γ'-CH_3	0.99 (d, 7.0 Hz)	19.4	
		β-CH	2.27 (m)	31.9	
		α-CH	3.61 (d, 4.5 Hz)	63.5	
		COOH	\	177.1	
5	threonine	CH_3	1.33 (d, 6.6 Hz)	22.4	TOCSY, HSQC, HMBC
		α-CH	3.59 (d, 4.8 Hz)	63.3	
		β-CH	4.27 (m)	69.0	
		COOH	\	175.3	
6	alanine	β-CH_3	1.48 (d, 7.3 Hz)	19.1	TOCSY, HMBC
		α-CH	3.78 (q, 7.3 Hz)	53.3	
		COOH	\	177.5	
7	lysine	γ-CH_2	1.45 (m), 1.51 (m)	24.6	TOCSY, HSQC
		δ-CH_2	1.72 (m)	27.4	
		β-CH_2	1.91 (m)	29.6	
		ε-CH_2	3.02 (t, 7.3 Hz)	38.6	
		α-CH	3.77 (t, 5.1 Hz)	53.5	
8	acetate	CH_3	1.92 (s)	26.5	HSQC, HMBC
		COOH	\	177.6	
9	glutamate	β-CH_2	2.02 (m), 2.09 (m)	30.0	TOCSY, HSQC
		γ-CH_2	2.34 (m)	36.2	
		α-CH	3.75 (m)	57.4	
10	citrate	α, α′CH_2	2.55 (d, 15.7 Hz)	48.3	TOCSY, HMBC
		γ, $\gamma'CH_2$	2.68 (d, 15.7 Hz)	48.3	
11	aspartate	β-CH	2.68 (dd, 7.6, 16.5 Hz)	37.6	TOCSY, HSQC, HMBC
		β'-CH	2.80 (dd, 3.8, 17.5 Hz)	37.6	
		α-CH	3.89 (dd, 3.6, 7.6 Hz)	55.2	
		γ-COOH	\	176.9	
		COOH	\	180.3	
12	asparagine	β-CH	2.87 (dd, 7.6, 16.5 Hz)	36.8	TOCSY, HSQC, HMBC
		β'-CH	2.95 (dd, 4.6, 16.5 Hz)	36.8	
		α-CH	4.00 (dd, 4.6, 7.6 Hz)	54.6	
		γ-$CONH_2$	\	177.5	
		COOH	\	175.9	
13	γ-aminobutyrate	2 CH	2.30 (t, 7.6 Hz)	37.1	TOCSY, HSQC, HMBC
		3 CH_2	1.91 (m)	26.6	
		4 CH_2	3.02 (t, 7.3 Hz)	42.4	
		COOH	\	184.4	
14	choline	N-$(CH_3)_3$	3.20 (s)	56.7	TOCSY, HSQC, HMBC
		O−CH_2	4.07 (m)	70.3	
		N−CH_2	3.52 (m)	\	

dx.doi.org/10.1021/pr101095t |*J. Proteome Res.* 2011, 10, 2273–2285

Table 1. Continued

no.	metabolites	group	δ ^{1}H (multiplicity)[a]	δ ^{13}C	experiments
15	phosphocholine	N-$(CH_3)_3$	3.23 (s)	56.7	TOCSY, HSQC
		O−CH_2	4.23 (m)	\	
		N−CH_2	3.61 (m)	\	
16	betaine	CH_3	3.26 (s)	56.7	TOCSY, HSQC, HMBC
		CH_2	3.91 (s)	68.9	
		COOH	\	176.9	
17	β-glucose	1 CH	4.65 (d, 8.0 Hz)	99.0	TOCSY, HSQC
		2 CH	3.25 (dd, 1.5, 8.0 Hz)	76.8	
		3 CH	3.49 (m)	78.6	
		4 CH	3.42 (m)	70.7	
		5 CH	3.47 (m)	77.8	
		6, 6′-CH	3.73, 3.90 (m)	63.8	
18	trehalose	1 CH	5.19 (d, 3.8 Hz)	96.2	TOCSY, HSQC
		2 CH	3.65 (dd, 3.8, 9.9 Hz)	79.7	
		3 CH	3.86 (dd, 2.2, 4.9 Hz)	75.8	
		4 CH	3.46 (t, 9.5 Hz)	72.5	
		5 CH	3.83 (m)	75.1	
		6,6′ CH	3.89 (dd, 2.3, 12.4 Hz)	65.6	
19	α-glucose	1 CH	5.24 (d, 3.7 Hz)	94.9	TOCSY, HSQC
		2 CH	3.53 (dd, 3.8, 9.8 Hz)	72.5	
		3 CH	3.73 (m)	73.8	
		4 CH	3.42 (m)	70.7	
		5 CH	3.86 (m)	72.5	
		6,6′ CH	3.74, 3.83 (m)	61.5	
20	sucrose	G-1 CH	5.42 (d, 3.9 Hz)	94.9	TOCSY, HSQC
		G-2 CH	3.56 (m)	72.9	
		G-3 CH	3.77 (m)	73.4	
21	GlcNAc-1-P[b]	1 CH	5.46 (dd, 3.5, 7.4 Hz)	96.6	TOCSY, HMBC
		2 CH	3.78 (m)	\	
		3 CH	3.46 (m)	\	
22	UDPG[b]	1 CH	5.59 (t, 5.5 Hz)	97.0	TOCSY, HMBC
		10 CH	4.36 (m)	\	
		11CH	5.95 (d, 8.0 Hz)	105.3	
		13 CH	5.97 (d, 8.0 Hz)	91.1	
		12 CH	7.94 (d, 8.0 Hz)	144.3	
		NH	8.34 (d, 8.4 Hz)	\	
23	uracil	5 CH	5.80 (d, 7.7 Hz)	103.7	TOCSY, HSQC
		6 CH	7.54 (d, 7.6 Hz)	147.5	
24	uridine	11 CH	7.88 (d, 8.0 Hz)	144.8	TOCSY, HSQC, HMBC
		12 CH	5.90 (d, 8.1 Hz)	104.9	
		7 CH	5.92 (d, 4.5 Hz)	91.6	
		6 CH	4.36 (t, 4.9 Hz)	87.0	
25	5′-UMP	12 CH	5.99 (d, 3.4 Hz)	105.3	TOCSY, HSQC
		7 CH	6.00 (d, 3.7 Hz)	90.4	
		11 CH	8.11 (d, 7.6 Hz)	142.7	
		6 CH	4.42 (m)	73.7	
26	fumarate	2,3 CH	6.52 (s)	136.5	TOCSY, HMBC
		COOH	\	177.3	
27	tyrosine	3,5 CH, ring	6.90 (d, 8.5)	118.4	TOCSY, HSQC
		2,6 CH, ring	7.20 (d, 8.5)	133.4	
		β-CH_2	3.05 (dd, 7.8, 14.8 Hz), 3.15 (dd, 8.6, 14.5 Hz)	39.4	
		α-CH	3.93 (m)	59.1	
		COOH	\	176.9	

dx.doi.org/10.1021/pr101095t |J. Proteome Res. 2011, 10, 2273–2285

Table 1. Continued

no.	metabolites	group	δ ^{1}H (multiplicity)[a]	δ ^{13}C	experiments
28	histidine	4 CH, ring	7.09 (s)	119.8	TOCSY, HSQC
		2 CH, ring	7.92 (s)	138.6	
		β-CH_2	3.20(dd, 5.1, 14.7 Hz), 3.25 (dd, 9.4, 14.6 Hz)	30.5	
		α-CH	4.00 (m)	56.6	
		COOH	\	174.4	
29	phenylalanine	4 CH, ring	7.33 (m)	132.3	TOCSY, HSQC
		3,5 CH, ring	7.38 (m)	130.6	
		2,6 CH, ring	7.43 (m)	132.1	
		β-CH_2	3.12 (dd,7.9, 14.9 Hz), 3.25 (dd, 5.2, 14.6 Hz)	39.4	
		α-CH	4.00 (m)	59.2	
30	tryptophan	6 CH, ring	7.29 (t, 7.4 Hz)	120.6	TOCSY, HSQC, HMBC
		7 CH, ring	7.53 (d, 8.3 Hz)	114.5	
		4 CH, ring	7.74 (d, 8.1 Hz)	120.6	
		β-CH_2	3.31 (dd,4.9, 14.3 Hz), 3.48 (dd, 9.1, 14.0 Hz)	26.4	
		α-CH	4.05 (m)	56.6	
		COOH	\	176.6	
31	guanosine	CH	8.01 (s)	138.6	TOCSY, HSQC, HMBC
		5′-CH_2	5.90 (d, 5.6 Hz)	90.8	
		4′-CH	4.41 (dd, 3.9, 9.1 Hz)	72.4	
		3′-CH	4.23 (m)	88.5	
32	adenosine	14 CH	8.33 (s)	143.1	TOCSY, HSQC
		8 CH	8.22 (s)	\	
		1 CH	6.06 (d, 6.3 Hz)	91.1	
33	formate	CH	8.46 (s)	\	JRES, TOCSY
34	NMNA[b]	2 CH	9.13 (s)	\	TOCSY, HSQC
		6 CH	8.84	\	
		1 CH_3	4.44 (s)	\	
35	inosine	2 CH	6.10 (d, 5.7 Hz)	\	JRES, TOCSY
		7 CH	8.24 (s)	\	
		12 CH	8.35 (s)	\	
36	hypoxanthine	2 CH	8.20 (s)	\	JRES, TOCSY
		7 CH	8.22 (s)	\	
37	malonate	CH2	3.12 (s)	73.7	HSQC
38	dimethylamine	CH_3	2.72 (s)	39.6	HSQC
39	methionine	γ-CH_2	2.65 (t, 7.5 Hz)	32.0	TOCSY, HSQC
		β-CH_2	2.17 (m)	32.5	
		α-CH	3.78 (m)	56.7	
		δ-CH_3	2.14 (s)	16.7	
		COOH	\	176.4	
40	propionate	CH_3	1.06 (t, 7.3 Hz)	19.4	TOCSY, HSQC
		CH_2	2.19 (q, 4.0 Hz)	\	
41	quinone[b]	CH	6.80 (s)	\	JRES, TOCSY
42	dTMP[b]	CH	7.87 (s)	139.4	TOCSY, HSQC
43	α-ketoglutarate	β-CH_2	2.45 (t, 7.9 Hz)	34.1	TOCSY, HSQC
		γ-CH_2	3.02 (t, 8.5 Hz)	42.3	
44	succinate	CH_3	2.41 (s)	36.7	HSQC, HMBC
		COOH	\	180.6	
45	pyruvate	CH_3	2.37 (s)	29.7	HSQC
46	glycine	CH_2	3.57 (s)	44.5	TOCSY, HSQC, HMBC
		COOH	\	177.1	
47	1,3-dimethyluracil[b]	5 CH	5.88 (d, 7.7 Hz)	\	JRES

Table 1. Continued

no.	metabolites	group	δ ^{1}H (multiplicity)[a]	δ ^{13}C	experiments
		6 CH	7.54 (d, 7.6 Hz)	\	
48	malate	α-CH	4.31 (dd, 3.1, 10.2 Hz)	73.5	TOCSY, HSQC, HMBC
		β-CH	2.68 (dd, 3.1, 15.4 Hz)	45.4	
		β'-CH	2.37 (dd, 10.2,15.4 Hz)	45.4	
		COOH	\	180.3	
49	glutamine	β-CH_2	2.14 (m)	30.0	TOCSY, HSQC, HMBC
		γ-CH_2	2.45 (m)	33.9	
		α-CH	3.79 (m)	57.5	
		C═O	\	175.8	
		COOH	\	177.5	
50	proline	α-CH	4.14 (m)	64.2	TOCSY, HSQC, HMBC
		β-CH_2	2.36 (m)	32.1	
		γ-CH_2	2.02 (m)	26.7	
		δ-CH_2	3.37 (m), 3.41 (m)	49.2	
		COOH	\	177.3	
51	arginine	γ,γ'-CH	1.68 (m), 1.72 (m)	24.4	TOCSY, HMBC, HSQC
		β-CH_2	1.91 (m)	29.3	
		δ-CH_2	3.25 (m)	42.4	
		α-CH	3.78 (t, 4.7 Hz)	57.3	
52	xanthine		7.76 (s)	\	
53	U1	\	7.59, 6.99, 6.39	\	COSY, TOCSY
54	U2	\	7.56, 6.37	\	COSY, TOCSY
55	ascorbate	\	4.50 (d, 1.9 Hz)	98.6	COSY, TOCSY, HSQC
		\	3.73 (m)	\	
56	syllo-inositol	CH	3.30 (s)	\	COSY, TOCSY
57	myo-inositol	2-CH	4.07 (t, 2.4 Hz)	75.2	TOCSY, HSQC, HMBC
		1,3 CH	3.52 (dd, 3.7, 9.8 Hz)	75.4	
		4,6 CH	3.61 (t, 4.4 Hz)	73.8	
		5 CH	3.29 (t, 4.5 Hz)	77.3	
58	nicotinic acid	2 CH	8.64 (d, 2.0 Hz)	153.2	TOCSY, HSQC, HMBC
		3 CH	7.60 (dd, 5.1, 7.6 Hz)	127.9	
		4 CH	8.06 (dt, 1.9, 8.2 Hz)	140.3	
59	guanidoacetate	\	3.80 (s)	\	JRES, TOCSY
60	U3	\	3.70 (s)	\	JRES, TOCSY
61	U4	\	6.14, 6.68	\	COSY, TOCSY

[a] Multiplicity: s, singlet; d, doublet; dd, doublet of doublets; t, triplet; q, quartet; U, unidentified signal; \, signals or multiplicities were not determined. [b] tentatively assigned; GlcNAc-1-P, N-acetylglucosamine-1-phosphate; UDPG, uridine diphosphate glucose; NMNA, N-Methylnicotinamide.

The loadings generated from the OPLS-DA results were plotted with an in-house developed MATLAB (v.7.0.14) script. In such case, loadings were back-transformed[43] and color-coded with correlation coefficients for all variables with hot colored (e.g., red) variables contributing more significantly to classification than the cold colored (e.g., blue) ones. The quality of 7-fold cross-validated OPLS-DA models was assessed with values of R^2X representing the total explained metabolic variables and of Q^2 indicating the predictability of the models. The model qualities were further evaluated by rigorous permutation tests with the permutation number of 200 (Figure S2). With $n = 18$ in this study, a cutoff value of 0.46 (i.e., $|r| > 0.46$) for correlation coefficients was used for the statistical significance based on the discrimination significance at the level of $p < 0.05$, which was determined according to the discriminating significance of the Pearson's product-moment correlation coefficient.[44]

Quantitative Analysis of Metabolites

Metabolite concentrations of *F. graminearum* strains 5035 and *Tri5*$^-$ were also calculated from the integrals of selected metabolite NMR signals (nonoverlapping ones) relative to that of internal reference (TSP) with known concentrations taking into consideration of relaxation times, T_1 (Table S1), as previously described.[28,34] These values were tabulated in Table 2. All the obtained metabolite concentrations were also subjected to statistical analyses (one way-ANOVA) using SAS V8 (Statistics Analysis System, SAS Institute) software.

RNA Isolation and Reverse Transcription Reaction

Total RNA of mycelium was isolated with Trizol reagent (Invitrogen). RNA samples were then treated with RNase-free DNase (Takara, Dalian, China) and ethanol-precipitated, followed by reverse-transcription with Superscript II (Invitrogen) and an oligo-dT_{20} primer.

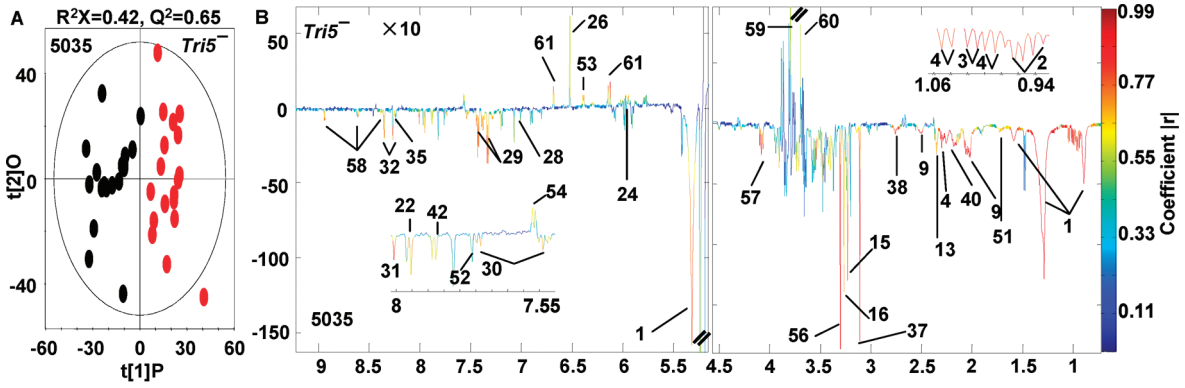

Figure 3. OPLS-DA results for the fungal extracts from *F. graminearum* strains 5035 (black dot) and *Tri5*$^-$ (red dot), n = 18. (A) Scores plot; (B) coefficient-coded loadings plot. The color scales showed correlation coefficients of metabolite variations. Metabolite key: 1, lipid; 2, leucine; 3, isoleucine; 4, valine; 9, glutamate; 13, γ-aminobutyrate; 15, phosphocholine; 16, betaine; 22, UDPG; 24, uridine; 26, fumarate; 29, phenylalanine; 30, tryptophan; 31, guanosine; 32, adenosine; 35, inosine, 37, malonate; 38, dimethylamine; 40, propionate; 42, dTMP; 51, arginine; 52, xanthine; 56, syllo-inositol; 57, myo-inositol; 58, nicotinic acid, 59, guanidoacetate.

Quantitative Real-Time PCR

Quantitative real-time PCR (qRT-PCR) reactions were carried out in a volume of 20 μL containing Sybr Greeen I PCR Master Mix (Toyobo, Osaka, Japan), 2 pmol each of forward and reverse gene-specific primers, and 5-μL of cDNA (1:50 dilution) derived from the above-mentioned reverse transcriptions. Gene-specific primers (Table S2) were designed using Primer Premier5 software (PREMIER Biosoft International) and genome sequence of *F. graminearum* http://www.broadinstitute.org/annotation/genome/fusarium_graminearum/MultiHome.html). PCR amplification was performed in an iQ5 Cycler (Bio-Rad) under the following conditions: 95 °C for 5 min, followed by 40 cycles of 95 °C for 20 s, 60 °C for 20 s, 72 °C for 20 s. The plate read was at 80 °C for 15 s. A melting curve was also performed to determine the specificity of each PCR primer by decreasing the reaction to 55 °C, and then increasing to 95 °C at a rate of 0.5 °C/10 s. To normalize the total amounts of cDNAs present in each reaction and to eliminate the intersample differences, a *F. graminearum* β-tubulin housekeeping gene was co-amplified as an external control. Three independent samples (biological replicates) were employed and the $2^{-\Delta\Delta C}{}_T$ method[45] was used to calculate the gene expression level for *F. graminearum* strains *Tri5*$^-$ and 5035 relative to β-tubulin. The data ($2^{-\Delta C}{}_T$) so obtained from qRT-PCR were subjected to the Student's t test and difference was considered significant with $p < 0.05$.

RESULTS

Mycotoxin Production of Two *Fusarium* Strains

The *Tri5*-deleted *Fusarium* strain, *Tri5*$^-$, was molecularly characterized[38] and displayed a normal rate of mycelial growth rate, hypha branch, conidiation, and ascorspore production as its wild-type counterpart 5035 (Figure 1). No trichothecene mycotoxins, DON and 15-ADON, were detected in the *Tri5*$^-$ strain, whereas the wild-type strain 5035 produced a large quantity of DON and 15-ADON under the same culture condition (Figure 1). A concomitant result was seen for the *Tri5* transcripts of the two isogenic strains. In addition, no other trichothecence mycotoxins, such as 3-ADON, NIV, FX, T2, or their derivatives, were detected in both strains (data not shown). This confirmed the successful deletion of *Tri5* gene for the *Tri5* $^-$ strain.

Metabolic Profiles of Two *Fusarium* Strains

Figure 2 shows ^{1}H NMR profiles of two *Fusarium* strains with more than 60 metabolites detected, including organic acids, sugars, amino acids, organic bases, betaine, cholines, pyrimidine, and purine metabolites. Among them, more than 50 metabolites were identified based on literature data[24,32,46,47] and in-house databases. The metabolite identifications were unambiguously confirmed with a series of 2D NMR experiments including ^{1}H−^{1}H COSY, TOCSY, ^{1}H−^{13}C HSQC, and HMBC. Their ^{1}H and ^{13}C signal information is tabulated in Table 1. Such assignments are sufficient for the purpose of this study even though some metabolites detected have not been unambiguously assigned at this stage (e.g., unknowns in Table 1). To obtain further details on the statistically significant metabonomic differences between two fungal strains, we performed multivariate data analyses on the NMR data from both strains.

Multivariate Data Analyses of the Metabolic Differences between Two Fungal Strains

PCA scores plot (Figure S1) showed that *Fusarium* strain *Tri5*$^-$ and wild-type 5035 were clearly clustered into two groups with two principal components, PC1 and PC3, explaining 71% variances in the data set. This suggests that these two strains may have distinct metabonomic differences due to *Tri5*-gene deletion. To further investigate which metabolites or pathways were significantly affected by dysfunctioning *Tri5* gene, an OPLS-DA model was constructed with metabolite profile data as **X**-matrix and group information as **Y**-matrix.[29,42] The scores plot from OPLS-DA (Figure 3A) showed that samples from two fungal strains clearly clustered into two separate groups with good model quality indicated by the values of model parameters (R^2X, 0.42; Q^2, 0.65). Coefficient-coded loadings plot (Figure 3B) indicated that these two strains had significant different metabolite compositions. Compared to the wild-type *Fusarium* 5035, *Tri5*$^-$ had significantly higher contents in guanidoacetate and fumarate but lower levels in lipids, glutamate (Glu), valine (Val), alanine (Ala), leucine (Leu), isoleucine (Ile), γ-aminobutyrate (GABA), and histidine (His). *Tri5*$^-$ also had lower levels in inositols (*myo*-inositol and *syllo*-inositol), choline metabolites (choline, phosphocholine and betaine), shikimate metabolites (tyrosine, phenylalanine and tryptophan), and pyrimidine and

Table 2. Metabolite Contents and Correlation Coefficients for *F. graminearum* Strains 5035 and *Tri5*$^-$

	coefficient (r)[a]	absolute content (mg/g)[b]	
metabolite (number in Table 1)	*Tri5*$^-$/5035	*Tri5*$^-$	5035
guanidoacetate (59)	0.58	–	–
fumarate (26)	0.52	0.11 ± 0.03[c]	0.08 ± 0.03
alanine (6)	−0.15	4.68 ± 1.35	5.32 ± 1.88
β-glucose (17)	−0.15	19.9 ± 2.27	20.68 ± 2.61
α-glucose (19)	−0.17	16.91 ± 1.97	17.86 ± 2.32
trehalose (18)	−0.26	112.2 ± 15.1	113.9 ± 12.4
citrate (10)	−0.44	2.51 ± 0.46	2.70 ± 0.40
glutamate (9)	−0.60	8.09 ± 1.12	8.72 ± 1.12
leucine (2)	−0.72	–	–
isoleucine (3)	−0.79	0.73 ± 0.11[c]	0.95 ± 0.13
valine (4)	−0.68	0.81 ± 0.11[c]	1.01 ± 0.14
arginine (51)	−0.46	–	–
γ-aminobutyrate (13)	−0.78	1.54 ± 0.26	1.69 ± 0.35
histidine (28)	−0.52	0.54 ± 0.08	0.61 ± 0.08
myo-inositol (57)	−0.80	–	–
syllo-inositol (56)	−0.79	1.42 ± 0.16[c]	1.80 ± 0.28
betaine (16)	−0.64	1.91 ± 0.19[c]	2.27 ± 0.31
phosphocholine (15)	−0.72	–	–
tyrosine (27)	−0.57	0.47 ± 0.07	0.52 ± 0.07
phenylalanine (29)	−0.71	0.51 ± 0.07[c]	0.63 ± 0.08
tryptophan (30)	−0.68	0.39 ± 0.05[c]	0.45 ± 0.05
uridine (24)	−0.49	0.18 ± 0.06	0.20 ± 0.06
malonate (37)	−0.80	5.47 ± 0.63[c]	6.89 ± 1.07
adenosine (32)	−0.74	0.37 ± 0.09[c]	0.54 ± 0.11
guanosine(31)	−0.74	0.12 ± 0.02[c]	0.14 ± 0.02
dTMP (42)	−0.53	–	–
xanthine (52)	−0.48	–	–
dimethylamine (38)	−0.78	–	–
propionate (40)	−0.84	–	–
UDPG (22)	−0.67	–	–
lipid (1)	−0.83	–	–

[a] The coefficients from OPLS-DA results; positive and negative signs represent positive and negative correlation in the concentrations, respectively. The coefficient of 0.46 was used as the cutoff value for the significant difference evaluation ($p < 0.05$). –, the absolute content was not determined in the corresponding extracts. [b] Average concentration and standard deviation (mean SD, mg/g of dried fungal material) were obtained from 18 independent samples of 5035 and *Tri5*$^-$, respectively, and each sample came from three dishes. [c] Significant difference compared with 5035 by one-way ANOVA analysis ($p < 0.05$).

purine metabolites (uridine, malonate, xanthine, guanosine and adenosine) (Figure 3B and Table 2).

Quantitative RT-PCR Analysis for Genes Involved in the Pathways of Altered Metabolites

To obtain regulation information on 25 key genes regulating the metabolic pathways of the above altered metabolites, quantitative real-time PCR (qRT-PCR) analyses were also performed with cDNA reverse-transcribed from mRNA isolated from two strains and a set of selected primers (Table S2). These primers were chosen on the basis of the differences of metabolic compounds detected between two strains and reported fungal metabolic pathways. The expression results showed (Figure 4) that two genes displayed an enhanced expression while eight genes displayed a reduced expression upon *Tri5* gene deletion. The gene encoding fumarate hydratase (*FH*) catalyzing conversion of fumarate to malate was significantly up-regulated (about 1.4-fold). The major facilitator superfamily hexose transporter gene (*MFSHT*) responsible for transportation of hexose also showed significant up-regulation (more than 2-fold) in the strain *Tri5*$^-$.

In contrast, eight genes showed significant down-regulations in the strain *Tri5*$^-$ compared to these in the strain 5035 relating to GABA shunt and metabolisms of shikimate, choline, and carbohydrates. Genes encoding citrate synthase (*CS*), glucose-6-phosphate-1-dehydrogenase (*G6PD*), and γ-aminobutyrate amino transferase (*GABAT*) showed more than 50% down-regulations, while the gene encoding NAD-dependent glutamate dehydrogenase (NAD^+-*GDH*) showed about 20% down-regulation in the strain *Tri5*$^-$. Furthermore, compared to the strain 5035, *Tri5*$^-$ had less transcripts for genes encoding glutamine synthetase (*GS*, 35%), 4-hydroxyphenylpyruvate dioxygenase (*HPPD*, 23%), betaine-aldehyde dehydrogenase (*BADH*, 16%), and putative sugar transporter (*PST*, 47%). The remaining 15 genes showed no significant difference of transcripts between the strains *Tri5*$^-$ and 5035 at the level of $p = 0.05$.

DISCUSSION

The trichothecene mycotoxins produced by *F. graminearum* such as DON and 15-ADON are known to be toxic to eukaryotes, including animals, humans, plants, and yeast, due to their inhibitory effects on protein synthesis.[8,9,48] The mycotoxin-producing *Fusarium* fungi themselves are believed to be self-protected from the toxicity due to the presence of an endogenous 3-*O*-acetyltransferase encoded by *Tri101*.[20] However, the biological and physiological role of the mycotoxins in the mycotoxin-producing fungi *in vivo* has long been a mystery ever since the identification of the mycotoxin compounds from the fungal species. Whether *Tri5* gene responsible for mycotoxin biosynthesis has any other functions is also an interesting topic.

This study showed that *Tri5*-deletion induced alterations to the expression of a number of other genes and systems-wide metabolic networks including GABA shunt, TCA cycle, metabolisms of choline, shikimate, pyrimidine, and purine (Figure 5) although the deletion of *Tri5* gene was only believed to be associated with the blockage of the mycotoxin biosynthesis previously. Such effects on GABA shunt were reflected with a down-regulation of *GS* and *GABAT* genes and concomitant reduction of glutamate together with depletion of GABA. *Tri5* deletion further induced changes in TCA intermediates such as fumurate together with expressional changes for *FH*, NAD^+-*GDH*, and *GS* genes. This implies that changes of these two pathways may be interlinked through α-ketoglutarate, which is involved in synthesis of glutamate. This is not surprising since TCA is essential for many key reactions and functions in organisms under pathogenic virulence.[49]

Furthermore, *Tri5* gene regulated trichodiene synthase catalyzes conversion of farnesyl pyrophosphate (FPP), which is an intermediate in the HMG-CoA reductase pathway, to trichodiene (TDN) that serves as the first intermediate entering into thichothecene mycotoxin biosynthesis.[15,16] Biosynthesis of thichothecene mycotoxins is in effect closely related to acetyl-CoA through 3-hydroxy-3-methylglutaryl-CoA (HMG-CoA) in the

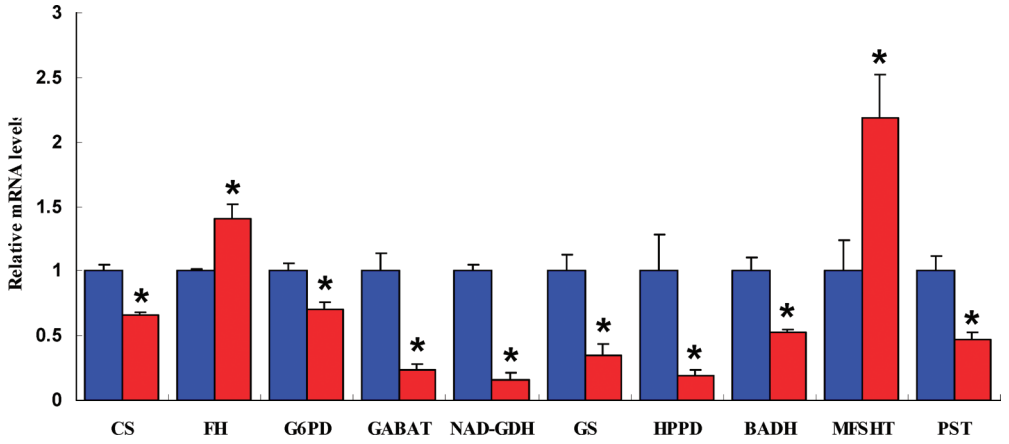

Figure 4. Quantitative real-time PCR data for the mRNA expression levels of *CS*, *FH*, *G6PD*, *GABAT*, *NAD*$^+$*-GDH*, *GS*, *HPPD*, *BADH*, *MFSHT*, and *PST* genes in *F. graminearum* strains 5035 and *Tri5*$^-$. Values represented relative mRNA levels against 5035 (whose values were set to unity). Asterisks (*) indicated significant differences ($p < 0.05$). Key: *CS*, citrate synthase; *FH*, fumarate hydratase; *G6PD*, glucose-6-phosphate-1-dehydrogenase; *GABAT*, γ-aminobutyrate amino transferase; *NAD*$^+$*-GDH*, NAD$^+$ dependent glutamate dehydrogenase; *GS*, glutamine synthetase; *BADH*, betaine-aldehyde dehydrogenase; *HPPD*, 4-hydroxyphenylpyruvate dioxygenase; *MFSHT*, major facilitator superfamily hexose transporter; *PST*, putative sugar transporter.

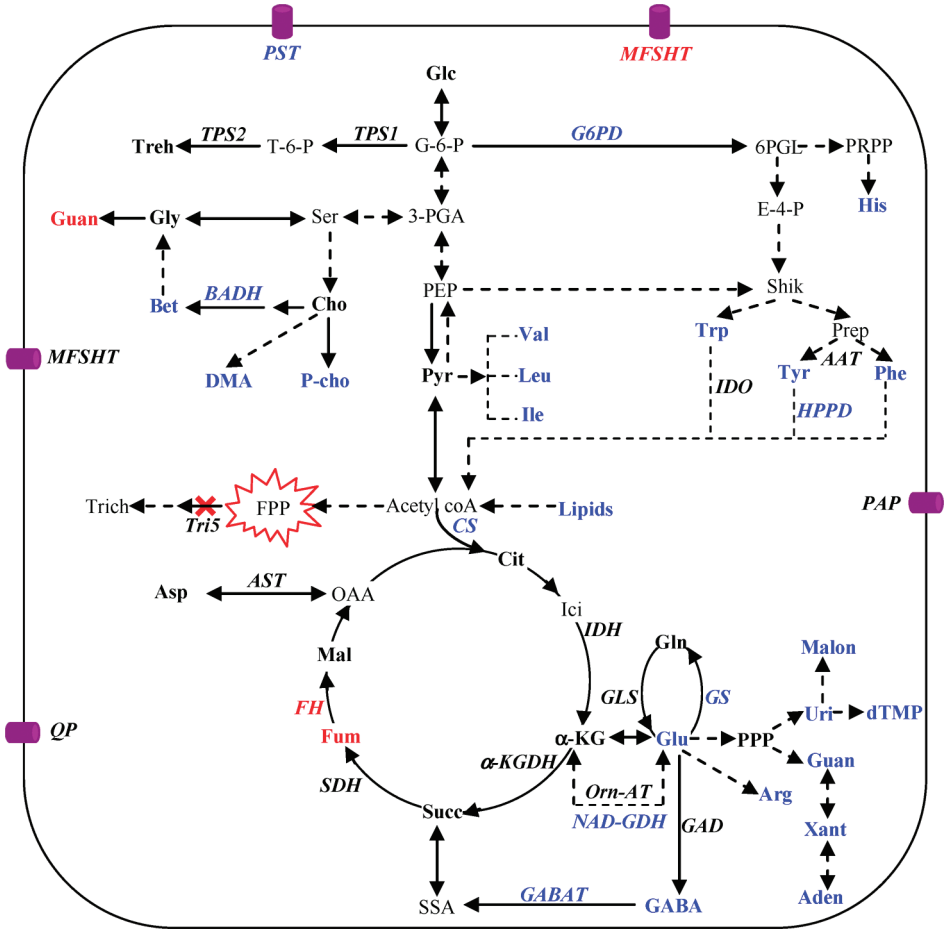

Figure 5. *Tri5* gene deletion caused metabolic changes in *F. graminearum*. Red colored symbols indicate significant up-regulations of metabolites and transcripts ($p < 0.05$), whereas blue colored symbols represent down-regulations of metabolites and transcripts ($p < 0.05$). Metabolites identified are shown in bold letters and genes with transcript measured are shown in italic and bold letters. Boxed *Tri5* with a red cross indicates a disruption of the *Tri5* gene leading to the blockage of FPP entering into trichothecene mycotoxin biosynthesis. Abbreviations for genes are as described in Table S2 and the abbreviations for metabolites are as described in the Abbreviations list.

dx.doi.org/10.1021/pr101095t |*J. Proteome Res.* 2011, 10, 2273–2285

mevalonate pathway. Acetyl-CoA is also related to the regulation of *CS* through TCA cycle and *HPPD* responsible for catabolism of tryptophan and phenylalanine as well. Therefore, the changes in TCA observed in this study may also be indirectly linked with the altered mycotoxin biosynthesis. Yet again, trichothecene mycotoxins produced naturally by *Fusarium* species seem to play a direct or indirect role in the fungal physiology and development even though details for such warrant further molecular biological investigations.

The *Tri5*-deletion induced reduction of amino acids can be understood since these metabolites are closely related to FPP, the substrate of the trichodiene synthase enzyme, via acetyl-CoA or via oxaloacetate in TCA (Figure 5). It is likely that the blockage of trichothecene biosynthesis pathway combined with the hexose monophosphate pathway (HMP) compensate the pathway of downstream metabolisms. The downstream flux goes toward pyruvate-mediated amino acid biosynthesis. The significant elevation of *MFSHT* induced by *Tri5*-deletion indicates altered transportation of hexoses which can be directly catalyzed by hexokinase and enter HMP. This pathway may serve as an energy source since HMP is an important pathway to metabolize glucose (not via TCA) to produce NADPH.

Tri5-deletion caused changes in the metabolisms of both choline and inositols probably imply some alterations to functions of cell membrane since both choline and inositols are important components of cell membrane phospholipids. This is further implicated by the changes of lipid levels upon *Tri5*-gene deletion. Decreases of Tyr, Phe, and Trp levels may also be suggestive of alterations in shikimate-mediated secondary metabolisms since these amino acids are all important metabolites in shikimate pathway. The overall decreases of pyrimidine and purine metabolites may indicate the effects of Tri5 deletion on biosynthesis of DNA and RNA. These strongly suggest that some further analyses of lipidome and the shikimate-mediated secondary metabolisms are necessary for the future studies.

In conclusion, combined NMR-based metabonomic and qRT-PCR analyses revealed that deleting *Tri5*-gene caused widespread and significant changes in primary metabolism in *F. graminearum*, apart from mycotoxin biosynthesis, although *Tri5* gene was only believed to be responsible for encoding trichodiene synthase. These metabolic changes induced by *Tri5* gene deletion involved both carbon and nitrogen metabolisms including GABA shunt, TCA cycle, metabolisms of amino acids, lipids, choline, shikimate, pyrimidine, and purine. These results appeared to support a hypothesis about some possible functions of mycotoxins in fungal physiology and raised the necessity for some future detailed studies in lipid and shikimate related metabolisms with detailed molecular biological approaches. These findings may also provide useful information for dissecting mechanisms and regulations involved in the trichothecene mycotoxin biosynthesis pathway and for the development of new strategies for controlling FHB.

■ ASSOCIATED CONTENT

Supporting Information

T_1 values for the protons of some selected metabolites (Table S1), expression levels of 25 genes measured with qRT-PCR (Table S2), scores plot from the PCA for *F. graminearum* strains 5035 and *Tri5*$^-$ (Figure S1) and the permutation test results with 200 permutations (Figure S2) are available free of charge via the Internet at http://pubs.acs.org.

■ AUTHOR INFORMATION

Corresponding Author

*Huiru Tang: State Key Laboratory of Magnetic Resonance and Atomic and Molecular Physics, Wuhan Centre for Magnetic Resonance, Wuhan Institute of Physics and Mathematics, the Chinese Academy of Sciences, Wuhan 430071, China; tel, +86-27-87198430; fax, +86-27-87199291; e-mail, huiru.tang@wipm.ac.cn. Yu-Cai Liao: College of Plant Science and Technology, Huazhong Agricultural University, Wuhan 430070, P. R. China; tel, +86-27-87283008; fax, +86-27-87283008; e-mail, yucailiao@mail.hzau.edu.cn.

Author Contributions

#These authors contributed equally to the work.

■ ACKNOWLEDGMENT

We acknowledge financial supports from the National Basic Research Program of China (2009CB118806), National Natural Science Foundation of China (30571160, 30771337, 20825520, 20921004), Ministry of Science and Technology of China (2007AA10Z425), the Ministry of Agriculture of China (2008ZX08002-001, 2009ZX08002-001B) and Chinese Academy of Sciences (KSCX2-YW-N-033). We also thank Dr. Hang Zhu of Wuhan Institute of Physics and Mathematics for assistance in developing MATLAB scripts used for color-coded OPLS-DA coefficient plots, which was based on a script downloaded from http://www.mathworks.com/matlabcentral/fileexchange.

COSY, correlated spectroscopy; TOCSY, total correlation spectroscopy; HSQC, heteronuclear single-quantum coherence; HMBC, heteronuclear multiple bond correlation; NMR, nuclear magnetic resonance; T_1, spin−lattice relaxation time; TCA cycle, tricarboxylic acid cycle; Suc, sucrose; Glc, glucose; G-6-P, glucose-6-phosphate; 3-PGA, 3-phosphoglycerate; Cho, choline; Bet, betaine; Shik, shikimate; Pyr, pyruvate; Prep, prephenate; PEP, phosphoenolpyruvate; 6PGL, 6-phosphogluconate; E-4-P, erythrose-4-phosphate; Cit, citrate; Ici, isocitrate; Succ, succinate; α-KG, α-ketoglutarate; Fum, fumarate; Mal, malate; OAA, oxalacetic acid; SSA, succinate semialdehyde; GABA, γ-aminobutyric acid; *CS*, citrate synthase; T-6-P, trehalose-6-P; Treh, trehalose; Ser, serine; P-cho, phosphocholine; Uri, uridine; Malon, malonate; Trich, trichothecene; Leu, leucine; Val, valine; Ile, isoleucine; Trp, tryptophan; Tyr, tyrosine; Phe, phenylalanine; Arg, arginine; Guan, guanosine; Aden, adenosine; Xant, xanthine; PRPP, 5-phosphoribosyl diphosphate; DMA, dimethylamine; His, histidine; PPP, Pentose Phosphate Pathway

■ REFERENCES

(1) Goswami, R. S.; Kistler, H. C. Heading for a disaster: *Fusarium graminearum* on cereal crops. *Mol. Plant Pathol.* **2004**, *5*, 515–525.

(2) McMullen, M.; Jones, R.; Gallenberg, D. Scab of wheat and barley: a reemerging disease of devastating impact. *Plant Dis.* **1997**, *81*, 1340–1348.

(3) Parry, D. W.; Jenkinson, P.; Mcleod, L. Fusarium ear blight (scab) in small grain cereals: a review. *Plant Pathol.* **1995**, *44*, 207–238.

(4) Xu, X.; Parry, D. W.; Nicholson, W. P.; Thomsett, M. A.; Simpson, D.; Edwards, S. G.; Cooke, B. M.; Doohan, F. M.; Brennan, J. M.; Moretti, A.; Tocco, G.; Mule, G.; Hornok, L.; Giczey, G.; Tatnell, J.

Predominance and association of pathogenic fungi causing Fusarium ear blight in wheat in four European countries. *Eur. J. Plant Pathol.* **2005**, *112*, 143–154.

(5) Malz, S.; Grell, M. N.; Thrane, C.; Maier, F. J; Rosager, P.; Felk, A.; Albertsen, K. S.; Salomon, S.; Bohn, L.; Schäfer, W.; Giese, H. Identification of a gene cluster responsible for the biosynthesis of aurofusarin in the *Fusarium graminearum* species complex. *Fungal Genet. Biol.* **2005**, *42*, 420–443.

(6) Windels, C. E. Economic and social impacts of Fusarium head blight: Changing farms and rural communities in the Northern Great Plains. *Phytopathology* **2000**, *90*, 17–21.

(7) Starkey, D. E.; Ward, T. J.; Aoki, T.; Gale, L. R.; Kistler, H. C.; Geiser, D. M.; Suga, H.; Tóth, B.; Varga, J.; O'Donnell, K. Global molecular surveillance reveals novel *Fusarium* head blight species and trichothecene toxin diversity. *Fungal Genet. Biol.* **2007**, *44*, 1191–1204.

(8) Shifrin, V. I.; Anderson, P. Trichothecene mycotoxins trigger a ribotoxic stress response that activates c-Jun N-terminal kinase and p38 mitogen-activated protein kinase and induces apoptosis. *J. Biol. Chem.* **1999**, *274*, 13985–13992.

(9) Li, F.; Li, Y.; Luo, X.; Yoshizawa, T. Fusarium toxins in wheat from an area in Henan Province, PR China, with a previous human red mould intoxication episode. *Food Addit. Contam.* **2002**, *19*, 163–167.

(10) O'Donnell, K.; Kistler, H. C.; Tacke, B. K.; Casper, H. H. Gene genealogies reveal global phylogeographic structure and reproductive isolation among lineages of *Fusarium graminearum*, the fungus causing wheat scab. *Proc. Natl. Acad. Sci. U.S.A.* **2000**, *97*, 7905–7910.

(11) Gutleb, A. C.; Morrison, E.; Murk, A. J. Cytotoxicity assays for mycotoxins produced by Fusarium strains: a review. *Environ. Toxicol. Pharmacol.* **2002**, *11*, 309–320.

(12) Ward, T. J.; Bielawski, J. P.; Kistler, H. C.; Sullivan, E.; O'Donnell, K. Ancestral polymorphism and adaptive evolution in the trichothecene mycotoxin gene cluster of Phytopathogenic Fusarium. *Proc. Natl. Acad. Sci. U.S.A.* **2002**, *9*, 9278–9283.

(13) Grove, J. F. The trichothecenes and their biosynthesis. In *Fortschritte der Chemie organischer Naturstoffe/Progress in the Chemistry of Organic Natural Products*; Herz, W., Falk, H., Kirby, G. W., Eds.; Springer: Wien, New York, 2007; Vol. 88, pp 63−130.

(14) Schollenberger, M.; Drochner, W. Fusarium toxins of the scirpentriol subgroup: a review. *Mycopathologia* **2007**, *164*, 101–118.

(15) Desjardins, A. E.; Hohn, T. M.; McCormick, S. P. Trichothecene biosynthesis in Fusarium species: chemistry, genetics, and significance. *Microbiol. Rev.* **1993**, *57*, 595–604.

(16) Kimura, M.; Takeshi, T.; Naoko, T. A.; Shuichi, O.; Makoto, F. Molecular and genetic studies of Fusarium trichothecene biosynthesis: pathways, genes, and evolution. *Biosci. Biotechnol. Biochem.* **2007**, *71*, 2105–2123.

(17) Achilladelis, B.; Hanson, J. R. Studies in terpenoid biosynthesis-I. The biosynthesis of metabolites of *Tricothecium roseum*. *Phytochemistry* **1968**, *7*, 589–594.

(18) Desjardins, A. E.; Proctor, R. H.; Bai, G. H.; McCormick, S. P.; Shaner, G.; Buechley, G.; Hohn, T. M. Reduced virulence of trichothecene-nonproducing mutants of Gibberella zeae in wheat field tests. *Mol. Plant−Microbe lnteract.* **1996**, *9*, 775–781.

(19) Langevin, F.; Eudes, F.; Comeau, A. Effect of trichothecenes produced by *Fusarium graminearum* during Fusarium head blight development in six cereal species. *Eur. J. Plant Pathol.* **2004**, *110*, 735–746.

(20) Kimura, M.; Shingu, Y.; Yoneyama, K.; Yamaguchi, I. Features of *Tri101*, the trichothecene 3-O-acetyltransferase gene, related to the self-defense mechanism in *Fusarium graminearum*. *Biosci. Biotechnol. Biochem.* **1998**, *62*, 1033–1036.

(21) Lowe, R. G. T.; Allwood, J. W.; Galster, A. M.; Urban, M.; Daudi, A.; Canning, G.; Ward, J. L.; Beale, M. H.; Hammond-Kosack, K. E. A Combined ^{1}H nuclear magnetic resonance and electrospray ionization−mass spectrometry analysis to understand the basal metabolism of plant-pathogenic *Fusarium* spp. *Mol. Plant−Microbe Interact.* **2010**, *23*, 1605–1618.

(22) Nicholson, J. K.; Lindon, J. C.; Holmes, E. 'Metabonomics': understanding the metabolic responses of living systems to pathophysiological stimuli via multivariate statistical analysis of biological NMR spectroscopic data. *Xenobiotica* **1999**, *29*, 1181–1189.

(23) Tang, H.; Wang, Y. Metabonomics: a revolution in progress. *Prog. Biochem. Biophys.* **2006**, *33*, 401–417.

(24) Ding, L.; Hao, F.; Shi, Z.; Wang, Y.; Zhang, H.; Tang, H.; Dai, J. Systems biological responses to chronic perfluorododecanoic acid exposure by integrated metabonomic and transcriptomic studies. *J. Proteome Res.* **2009**, *8*, 2882–2891.

(25) Yap, I. K. S.; Clayton, T.; Tang, H. R.; Everett, J.; Hanton, G.; Provost, J.; LeNet, J.; Charuel, C.; Lindon, J.; Nicholson, J. An integrated metabonomic approach to describe temporal metabolic disregulation induced in the rat by the model hepatotoxin allyl formate. *J. Proteome Res.* **2006**, *5*, 2675–2684.

(26) Liu, C.; Hao, F.; Hu, J.; Zhang, W.; Wan, L.; Zhu, L.; Tang, H.; He, G. Revealing different systems responses to brown planthopper infestation for pest susceptible and resistant rice plants with the combined metabonomic and gene-expression analysis. *J. Proteome Res.* **2010**, *9*, 6774–6785.

(27) Grata, E.; Boccard., J.; Glauser, G.; Carrupt, P. A.; Farmer, E. E.; Wolfender, J. L.; Rudaz., S. Development of a two-step screening ESI-TOF-MS method for rapid determination of significant stress-induced metabolome modifications in plant leaf extracts: the wound response in *Arabidopsis thaliana* as a case study. *J. Sep. Sci.* **2007**, *30*, 2268–2278.

(28) Dai, H.; Xiao, C.; Liu, H.; Tang, H. Combined NMR and LC-MS analysis reveals the metabonomic changes in *Salvia Miltiorrhiza* Bunge induced by water depletion. *J. Proteome Res.* **2010**, *9*, 1460–1475.

(29) Xiao, C.; Dai, H.; Liu, H.; Wang, Y.; Tang, H. Revealing the metabonomic variation of rosemary extracts using ^{1}H NMR spectroscopy and multivariate data analysis. *J. Agric. Food. Chem.* **2008**, *56*, 10142–10153.

(30) Wang, Y.; Tang, H.; Holmes, E.; Lindon, J.; Turini, M.; Sprenger, N.; Bergonzelli, G.; Fay, L. B.; Kochhar, S.; Nicholson, J. K. Biochemical characterization of rat intestine development using high resolution magic-angle-spinning ^{1}H NMR spectroscopy and multivariate data analysis. *J. Proteome Res.* **2005**, *4*, 1324–1329.

(31) Abdel-Farid, I. B.; Jahangir, M.; van den Hondel, C. A. M. J. J.; Kim, H. K.; Choi, Y. H.; Verpoorte, R. Fungal infection-induced metabolites in *Brassica rapa*. *Plant Sci.* **2009**, *176*, 608–615.

(32) Zhang, X.; Wang, Y.; Hao, F.; Zhou, X.; Han, X.; Tang, H.; Ji, L. Human serum metabonomic analysis reveals progression axes for glucose intolerance and insulin resistance statuses. *J. Proteome Res.* **2009**, *8*, 5188–5195.

(33) Yang, Y.; Li, C.; Nie, X.; Feng, X.; Chen, W.; Yue, Y.; Tang, H.; Deng, F. Metabonomic studies of human hepatocellular carcinoma using high-resolution magic-angle spinning ^{1}H NMR spectroscopy in conjunction with multivariate data analysis. *J. Proteome Res.* **2007**, *6*, 2605–2614.

(34) Dai, H.; Xiao, C.; Liu, H.; Hao, F.; Tang, H. Combined NMR and LC-DAD-MS analysis reveals comprehensive metabonomic variations for three phenotypic cultivars of *Salvia Miltiorrhiza* Bunge. *J. Proteome Res.* **2010**, *9*, 1565–1578.

(35) Xiao, C.; Hao, F.; Qin, X.; Wang, Y.; Tang, H. An optimized buffer system for NMR-based urinary metabonomics with effective pH control, chemical shift consistency and dilution minimization. *Analyst* **2009**, *134*, 916–925.

(36) Wu, A.; Li, H.; Zhao, C.; Liao, Y. Comparative pathogenicity of *Fusarium graminearum* from China revealed by wheat coleoptile and floret inoculations. *Mycopathologia* **2005**, *160*, 75–83.

(37) Zhang, J.; Li, H.; Dang, F.; Qu, B.; Xu, Y.; Zhao, C.; Liao, Y. Determination of the trichothecene mycotoxin chemotypes and associated geographical distribution and phylogenetic species of the *Fusarium graminearum* clade from China. *Mycol. Res.* **2007**, *111*, 967–975.

(38) Li, X.; Zhang, J.; Song, B.; Li, H.; Xu, H.; Qu, B.; Dang, F.; Liao, Y. Resistance to Fusarium head blight and seedling blight in wheat is

associated with activation of a cytochrome P450 gene. *Phytopathology* **2010**, *100*, 183–191.

(39) Steele, G. C.; Trinci, A. P. J. Morphology and growth kinetics of hyphae of differentiated and undifferentiated mycelia of *Neurospora crassa*. *J. Gen. Microbiol.* **1975**, *91*, 362–368.

(40) Xu, Y.; Li, H.; Zhang, J.; Song, B.; Chen, F.; Duan, X.; Xu, H.; Liao, Y. Disruption of the chitin synthase gene *Chs1* from *Fusarium asiaticum* results in an altered structure of cell walls and reduced virulence. *Fungal Genet. Biol.* **2010**, *47*, 205–215.

(41) Wang, J.; Li, H.; Qu, B.; Zhang, J.; Huang, T.; Chen, F.; Liao, Y. Development of a generic PCR detection of 3-acetyldeoxynivalenol-, 15-acetyldeoxynivalenol- and nivalenol-chemotypes of *Fusarium graminearum* clade. *Int. J. Mol. Sci.* **2008**, *9*, 2495–2504.

(42) Trygg, J. O2-PLS for qualitative and quantitative analysis in multivariate calibration. *J. Chemom.* **2002**, *16*, 283–293.

(43) Wang, Y.; Lawler, D.; Larson, B.; Ramadan, Z.; Kochhar, S.; Holmes, E.; Nicholson, J. K. Metabonomic investigations of aging and caloric restriction in a life-long dog study. *J. Proteome Res.* **2007**, 1846–1854.

(44) Cloarec, O.; Dumas, M. E.; Trygg, J.; Craig, A.; Barton, R. H.; Lindon, J. C.; Nicholson, J. K.; Holmes, E. Evaluation of the orthogonal projection on latent structure model limitations caused by chemical shift variability and improved visualization of biomarker changes in ^{1}H NMR spectroscopic metabonomic studies. *Anal. Chem.* **2005**, *77*, 517–526.

(45) Livak, K. J.; Schmittgen, T. D. Analysis of relative gene expression data using real-time quantitative PCR and the $2^{-\Delta\Delta CT}$ method. *Methods* **2001**, *25*, 402–408.

(46) Fan, T. W. M. Metabolite profiling by one- and two-dimensional NMR analysis of complex mixtures. *Prog. Nucl. Magn. Reson. Spectrosc.* **1996**, *28*, 161–219.

(47) Fan, T. W. M.; Lane, A. N. Structure-based profiling of metabolites and isotopomers by NMR. *Prog. Nucl. Magn. Reson. Spectrosc.* **2008**, *52*, 69–117.

(48) Poppenberger, B.; Berthiller, F.; Lucyshyn, D.; Sieberer, T.; Schuhmacher, R.; Krska, R.; Kuchler, K.; Glossl, J.; Luschnig, C.; Adam, G. Detoxification of the Fusarium mycotoxin deoxynivalenol by a UDP-glucosyltransferase from *Arabidopsis thaliana*. *J. Biol. Chem.* **2003**, *278*, 47905–47914.

(49) Zhu, Y.; Xiong, Y.; Sadykov, M. R.; Fey, P. D.; Lei, M. G.; Lee, C. Y.; Bayer, A. S.; Somerville, G. A. Tricarboxylic acid cycle-dependent attenuation of *Staphylococcus aureus* in vivo virulence by selective inhibition of amino acid transport. *Infect. Immun.* **2009**, *77*, 4256–4264.